Research Square

Preprints are preliminary reports that have not undergone peer review.
They should not be considered conclusive, used to inform clinical practice,
or referenced by the media as validated information.

Dissolution of the collinear structure in the solar-sail circular restricted three-body problem: an exact tidal-parity threshold and a universal frequency bound

Bishwaswarup Nayak

bishwaswarup@iisc.ac.in

Indian Institute of Science Bangalore https://orcid.org/0009-0001-9926-5329

Research Article

Keywords: Solar sail, Restricted three-body problem, Photogravitational problem, Artificial equilibria, Collinear points, Legendre coefficient c2, Halo orbits, Controllability

Posted Date: October 6th, 2026

DOI: https://doi.org/10.21203/rs.3.rs-11257328/v1

License: This work is licensed under a Creative Commons Attribution 4.0 International License.
Read Full License

Additional Declarations: The authors declare no competing interests.

Dissolution of the collinear structure in the solar-sail circular restricted three-body problem: an exact tidal-parity threshold and a universal frequency bound

Bishwaswarup Nayak [1*]

[1*]Department of Physics, Indian Institute of Science, Bengaluru, 560012, Karnataka, India.

Corresponding author(s). E-mail(s): bishwaswarup@iisc.ac.in;

Abstract

A face-on solar sail does not displace the collinear Lagrange point of the circular restricted three-body problem; it dissolves it. Because the radiation force is radial and therefore conservative, it rescales solar gravity as $(1-\mu) \to (1-\beta)(1-\mu)$, and the on-axis equilibrium degenerates smoothly into a heliocentric hovering point as the lightness number β grows. We obtain two exact results. First, imposing *tidal parity*, the condition that the smaller primary's tidal term $s = \mu/r_2^3$ equal the centrifugal background, yields $\beta_{\rm crit} = 2\mu^{1/3} - \mu^{2/3}$, exact for every mass ratio and verified to machine precision over $\mu \in [10^{-7}, 10^{-2}]$; for Sun–Earth, $\beta_{\rm crit} = 0.0286$. Parity is the unique level of the family $s = \kappa$ at which the smaller primary drops out of the on-axis balance identically. Second, the ratio of the out-of-plane to in-plane linear frequencies at any collinear equilibrium is confined to $\nu/\omega \in [2\sqrt{2}/3,\, 1)$, with the bound attained at Legendre coefficient $c_2 = 8/5$, where $\lambda_u^2 : \nu^2 : \omega^2 = 7 : 8 : 9$. Both results are independent of μ, and the band contains no commensurability of denominator below 18, so neither marks a bifurcation: they are exact structural landmarks of a smooth degeneration. Parity corresponds to an instability e-folding time of 38.6 d at Sun–Earth and lies a factor of 4.6 beyond the best sail flown. Finally, at the face-on attitude the clock angle has no first-order authority, so the sail is a single-input system, uncontrollable for purely in-plane or purely vertical tilt and controllable otherwise because $\nu \neq \omega$.

Keywords: Solar sail, Restricted three-body problem, Photogravitational problem, Artificial equilibria, Collinear points, Legendre coefficient $\boldsymbol{c_2}$, Halo orbits, Controllability

1 Introduction

Artificial equilibria generated by continuous low thrust have been studied since McInnes *et al.* [1] mapped the surfaces of sail-displaced equilibria in the restricted three-body problem, and the periodic orbits about them are equally well established: Baoyin and McInnes [2] constructed halo orbits at the Sun–Earth artificial L_1, Waters and McInnes [3] treated families above the ecliptic, and Farrés and Jorba [4, 5] analysed the quasi-periodic dynamics and station-keeping in the same region. The standard reference remains [6]. With the sail face-on the problem is the photogravitational restricted problem, whose equilibria were classified by Simmons, McDonald and Brown [7]; the analogous artificial equilibria for general continuous low thrust were mapped by Morimoto *et al.* [8], and those of non-ideal (generalised) sails by Aliasi, Mengali and Quarta [9, 10], using refined optical force models [11, 12]. Closest to the present work, Verrier, Waters and Sieber [13] followed the L_1 halo family of exactly this face-on (radial) sail problem through β and found it reorganised by a branch point near $\beta \approx 0.0387$. Control at sail equilibria and periodic orbits has been treated by Bookless and McInnes [14, 15], Biggs *et al.* [16], Farrés and Jorba [17, 18] and Huang *et al.* [19], and mission concepts that use sub-L_1 artificial equilibria include Sunjammer [20] and Solar Cruiser [21]; Gong and Macdonald [22] review the technology.

What that literature supplies is numerical: the equilibrium abscissa is obtained by root-finding on the on-axis balance for each β, and the orbit families by Lindstedt–Poincaré expansion or numerical continuation. The equilibrium coordinates enter as computed inputs. What it does not supply is an algebraic characterisation of *how the collinear structure itself degrades* as β grows — at what sail performance the smaller primary ceases to organise the dynamics at all, and whether that point admits a closed form.

This paper supplies that characterisation. Our starting observation is that a face-on sail ($\alpha = 0$) exerts a purely radial and hence conservative force, so it does not perturb the collinear point: it rescales one primary's mass and the equilibrium migrates toward a *heliocentric hovering point* at which reduced solar gravity balances centrifugal acceleration at the synchronous rate. The three-body character of the equilibrium therefore does not shift, it decays, and the useful question is the rate and the scale of that decay.

Section 2 sets out the model and the conservative rescaling. Section 3 defines the saddle strength $s = \mu/r_2^3$ and measures its four-decade collapse. Section 4 derives the exact tidal-parity threshold, the paper's principal result, and validates it across five decades of mass ratio; Section 4.3 embeds it in a one-parameter hierarchy of tidal-strength levels and shows which property distinguishes it, and Section 4.4 reads it through the instability timescale a mission would actually feel. Section 5 establishes the frequency bound $\nu/\omega \in [2\sqrt{2}/3, 1)$, locates its exact extremum at $c_2 = 8/5$, and reports a systematic negative: no low-order resonance is attainable anywhere, which is what forbids interpreting either threshold as a bifurcation. Section 6 tracks the halo families across the flown sail band by pseudo-arclength continuation. Section 7 derives the sail control Jacobian and the singularity of the face-on nominal. Section 8 places β_{crit} against every sail flown to date. Section 9 states the limitations plainly.

On terminology.

We use *tidal parity* for the condition $s = 1$. The name is a label of convenience and carries no meaning beyond that definition. Likewise, the scale $\mu^{1/3}$ is not new — it is the Hill radius up to the factor $3^{1/3}$, and is standard in tidal-stability analysis [23, 24]. Our contribution is not the scale but the exact sail parameter required to place a spacecraft on it.

2 Model

We work in the usual synodic frame of the circular restricted three-body problem, non-dimensionalised so that the primary separation, the total mass and the mean motion are unity. The larger primary sits at $x = -\mu$ and the smaller at $x = 1 - \mu$, with $\mu = M_2/(M_1 + M_2)$. Distances from the primaries are

$$r_1 = \|\boldsymbol{r} - \boldsymbol{r}_1\|, \qquad r_2 = \|\boldsymbol{r} - \boldsymbol{r}_2\|, \tag{1}$$

and on the segment between them $r_1 = x + \mu$ and $r_2 = (1 - \mu) - x$, so that

$$r_1 + r_2 = 1 \quad \text{identically.} \tag{2}$$

Equation (2) is exact, not asymptotic, and is used in Section 4.

2.1 Sail acceleration

We model an ideal specular reflector. With α the cone angle between the Sun line and the sail normal and δ the clock angle about the Sun line,

$$\boldsymbol{a}_{\text{sail}} = \beta \frac{1-\mu}{r_1^2} \cos^2\alpha \, \hat{\boldsymbol{n}}, \qquad \hat{\boldsymbol{n}} = \cos\alpha \, \hat{\boldsymbol{r}} + \sin\alpha\cos\delta \, \hat{\boldsymbol{p}} + \sin\alpha\sin\delta \, \hat{\boldsymbol{q}}, \tag{3}$$

where β, the lightness number, is the ratio of the peak radiation-pressure acceleration to solar gravity. The force is directed along the normal with magnitude proportional to $\cos^2\alpha$; this is the specular reflector, and it is distinct from the perfect absorber, for which the force lies along the Sun line with magnitude proportional to $\cos\alpha$. The two coincide only at $\alpha = 0$.

The triad in (3) must be orthonormal. We take

$$\hat{\boldsymbol{r}} = \frac{\boldsymbol{r} - \boldsymbol{r}_1}{r_1}, \qquad \hat{\boldsymbol{p}} = \frac{\hat{\boldsymbol{k}} \times \hat{\boldsymbol{r}}}{\|\hat{\boldsymbol{k}} \times \hat{\boldsymbol{r}}\|}, \qquad \hat{\boldsymbol{q}} = \hat{\boldsymbol{r}} \times \hat{\boldsymbol{p}}, \tag{4}$$

with $\hat{\boldsymbol{k}}$ the out-of-ecliptic unit vector. Substituting $\hat{\boldsymbol{k}}$ itself for $\hat{\boldsymbol{q}}$ — a natural but incorrect shortcut — gives a non-orthonormal triad, since $\hat{\boldsymbol{r}} \cdot \hat{\boldsymbol{k}} = z/r_1 \neq 0$ off the ecliptic, and then $\|\hat{\boldsymbol{n}}\|^2 = 1 + \sin(2\alpha)\sin\delta\,(z/r_1)$, so that the nominal unit normal is not a unit vector and both the magnitude and the direction of the force are wrong. Since $\|\hat{\boldsymbol{n}}\|^2 - 1$ is maximised at $\sin(2\alpha)\sin\delta = 1$, the worst-case error in $\|\hat{\boldsymbol{n}}\|$ is 1.0 % at $z/r_1 = 0.02$ and 4.4 % at $z/r_1 = 0.09$. It vanishes identically at $\alpha = 0$, so no face-on

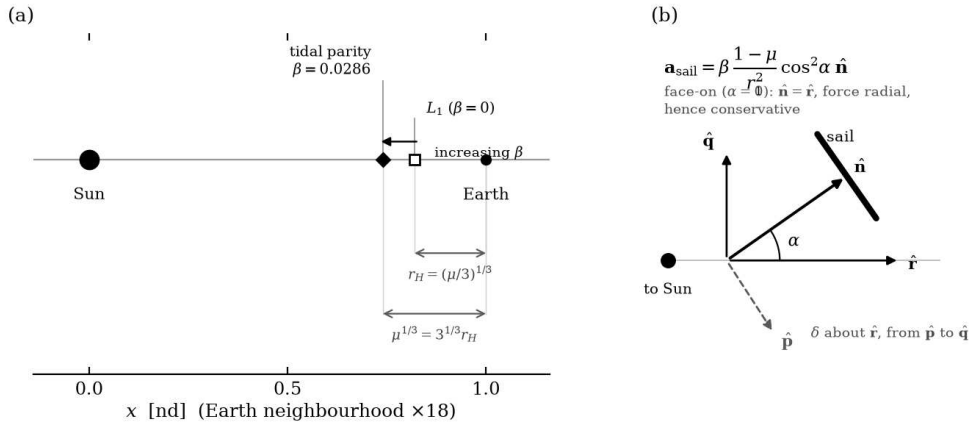


Fig. 1 Geometry of the face-on solar-sail CR3BP. **(a)** The synodic frame. The classical L_1 lies essentially on the Hill sphere ($r_2 = 0.9967\, r_H$); as β grows the equilibrium migrates sunward, reaching the tidal-parity radius $r_2 = \mu^{1/3} = 3^{1/3} r_H$ at $\beta = 0.0286$. The Earth neighbourhood is exaggerated by a factor of 18; at true scale every feature would collapse onto the smaller primary. **(b)** Attitude convention and the orthonormal triad (4). At $\alpha = 0$ the normal is $\hat{\boldsymbol{r}}$, the force is radial, and the sail is conservative.

result in this paper is affected; we record it because off-axis quantities computed on the shortcut triad are not reliable. Figure 1 shows the geometry.

2.2 The face-on case is conservative

Setting $\alpha = 0$ in (3) gives $\boldsymbol{a}_{\mathrm{sail}} = \beta(1-\mu) r_1^{-2} \hat{\boldsymbol{r}}$, a central force derivable from the potential $-\beta(1-\mu)/r_1$. It therefore merely rescales the larger primary, and the entire problem reduces to a CR3BP with modified pseudo-potential

$$U = \tfrac{1}{2}\left(x^2 + y^2\right) + \frac{(1-\beta)(1-\mu)}{r_1} + \frac{\mu}{r_2}. \tag{5}$$

A Jacobi integral survives,

$$C_{\mathrm{sail}} = 2U - v^2, \tag{6}$$

and it is U of (5), not the unscaled gravitational pseudo-potential, that must be used: the two differ by $2\beta(1-\mu)/r_1$, which varies along an orbit, so the gravitational Jacobi constant is not an integral for $\beta \neq 0$. On a representative family member ($\beta = 0.001$) we measure a spread of 1.8×10^{-15} in C_{sail} against 5.8×10^{-6} in its gravitational counterpart over one full period.

For $\alpha \neq 0$ the force acquires a transverse component, is no longer conservative, and no Jacobi integral exists. Every result in Sections 3–6 is therefore restricted to $\alpha = 0$; Section 7 is the sole exception and is explicitly a statement about the linearisation in the attitude angles.

3 Dissolution of the collinear structure

3.1 The hovering law

Deleting the smaller primary from (5) leaves an on-axis balance whose root is

$$x_{\mathrm{hover}}(\beta) = \big[(1-\beta)(1-\mu)\big]^{1/3}, \tag{7}$$

the radius at which reduced solar gravity balances centrifugal acceleration at the synchronous rate. This is a heliocentric hovering point, not a perturbed Lagrange point. The full three-body equilibrium satisfies

$$x = \frac{(1-\beta)(1-\mu)}{r_1^2} - \frac{\mu}{r_2^2}, \tag{8}$$

and the difference between its root and (7) is the smaller primary's entire contribution. At $\beta = 0.5$ that contribution is 3 817 km against a standoff of 30 865 449 km, i.e. 20.6 Hill radii: the Earth is dynamically irrelevant there, and results quoted at such β describe hovering geometry rather than three-body dynamics.

3.2 Linear structure and the saddle strength

Linearising (5) on the axis gives $U_{xx} = 1 + 2A$, $U_{yy} = 1 - A$, $U_{zz} = -A$ with

$$A(\beta) = \underbrace{\frac{(1-\beta)(1-\mu)}{r_1^3}}_{S} + \underbrace{\frac{\mu}{r_2^3}}_{s}. \tag{9}$$

This A is not a new quantity. Setting $\beta = 0$ and using $r_1 + r_2 = 1$, (9) reduces to $\mu/\gamma^3 + (1-\mu)/(1-\gamma)^3$ with $\gamma = r_2$, which is exactly the second Legendre coefficient c_2 of the collinear expansion introduced by Richardson [25] and used throughout halo-orbit theory [26, 27]. We verify the identity numerically to machine zero at Sun–Earth, Earth–Moon and Sun–Jupiter. We therefore write

$$A \equiv c_2, \tag{10}$$

and use c_2 from here on. The sail's effect is to replace $(1-\mu)$ by $(1-\beta)(1-\mu)$ in that coefficient: *a solar sail continuously detunes* c_2, which is otherwise fixed once the system and the libration point are chosen. This is the compact statement of what a sail contributes, and we return to it in Section 5.

The out-of-plane motion is a pure oscillator, $\nu = \sqrt{c_2}$. The in-plane characteristic polynomial is

$$\lambda^4 + (2 - A)\lambda^2 + \big(1 + A - 2A^2\big) = 0, \tag{11}$$

Table 1 Collapse of the saddle strength $s = \mu/r_2^3$ and of the unstable eigenvalue with sail lightness number, Sun–Earth ($\mu = 3.003 \times 10^{-6}$). Tidal parity is $s = 1$.

β	s	λ_u [nd]	note
0	3.030 3	2.532 56	classical L_1
0.010	2.123	2.138 31	
0.028646	1.000	1.505 42	tidal parity
0.050	0.401 2	0.994 49	
0.100	0.068 20	0.444 00	
0.500	3.419×10^{-4}	0.035 78	$20.6\,r_H$ standoff

whose roots are $\lambda^2 = \frac{1}{2}\big[(A-2) \pm D\big]$ with $D = \sqrt{A(9A-8)}$, giving a saddle exponent λ_u and a centre frequency ω,

$$\lambda_u^2 = \tfrac{1}{2}\big[(A-2) + D\big], \qquad \omega^2 = \tfrac{1}{2}\big[D - (A-2)\big]. \tag{12}$$

A real hyperbolic pair requires $c_2 > 1$.

As the equilibrium recedes from the smaller primary, $r_1^3 \to (1-\beta)(1-\mu)$ by (7) and hence $S \to 1$, so

$$c_2 - 1 \;\longrightarrow\; s = \frac{\mu}{r_2^3}. \tag{13}$$

We call s the *saddle strength*. Because $s > 0$ for all finite r_2, the saddle never strictly disappears: there is no bifurcation, only a smooth decay, and the physically meaningful statement is its rate. Table 1 records that rate, and s falls four decades between $\beta = 0$ and $\beta = 0.5$. Figure 5 shows the corresponding decline across the flown band for a fixed-amplitude halo orbit, whose largest Floquet multiplier falls from 1385 at $\beta = 0$ to 86 at $\beta = 0.05$.

It is worth being precise about (13), because the convergence is slower than it looks. At tidal parity, $S = (1-\mu)/(1-\mu^{1/3}) = 1.014635$ exactly, so $c_2 = 2.014635$ rather than 2, and $\lambda_u = 1.505418$ rather than $5^{1/4} = 1.495349$. The identification $c_2 - 1 = s$ carries an $O(\mu^{1/3})$ error, 0.73 % in c_2 at the Sun–Earth threshold. Both terms in (9) are nonetheless of smaller-primary origin: with the primary deleted, $S = 1$ identically, so $S-1$ measures its indirect effect through the displacement of the equilibrium, while s measures the direct tidal term. We therefore write $A - 1 = (S-1) + s$ and use the exact A throughout.

Two consequences of Figure 2(d) deserve emphasis, because both have been misread in the past. As $c_2 \to 1$ the planar roots of (11) become $\lambda^2 \in \{0, -1\}$ and $\nu = \sqrt{A} \to 1$, so the in-plane period is driven to exactly 2π in non-dimensional units — one year for Sun–Earth. This is *forced*, not resonant: in an inverse square field the epicyclic frequency equals the mean motion identically. Second, $\lambda_u \to 0$ does not indicate that the sail has stabilised a saddle; the orbit has simply moved away from one, and the residual instability is precisely the smaller primary's leftover tidal term.

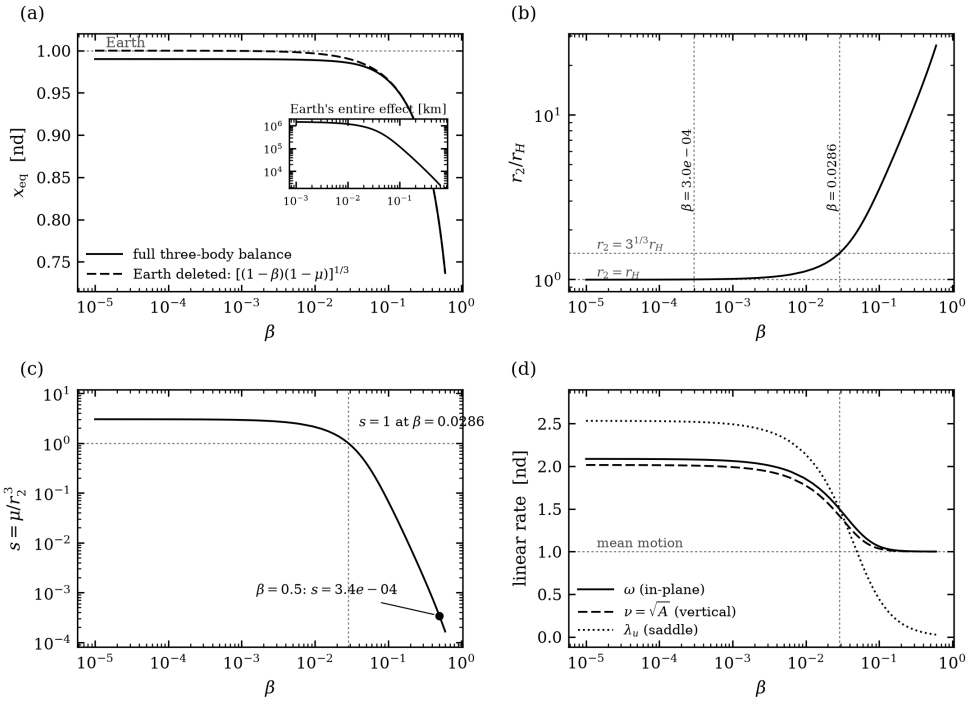


Fig. 2 Dissolution of the Sun–Earth collinear structure. **(a)** The full three-body equilibrium is indistinguishable from the Earth-free hovering law (7); the inset shows the smaller primary's entire contribution collapsing to a few thousand kilometres. **(b)** The standoff crosses the Hill sphere almost immediately (at $\beta = 2.98 \times 10^{-4}$, the Hill-exit value, not β_{crit}) and reaches $20.6\, r_H$ by $\beta = 0.5$. **(c)** The saddle strength falls four decades; $s = 1$ locates tidal parity. **(d)** Both frequencies converge on the mean motion and $\lambda_u \to 0$: the Keplerian epicyclic degeneracy of an inverse square field, not a resonance with the smaller primary.

4 The tidal-parity threshold in closed form

4.1 Derivation

Define tidal parity as the condition that the direct tidal term equal the centrifugal background of the synodic frame,

$$s = \frac{\mu}{r_2^3} = 1 \qquad \Longleftrightarrow \qquad r_2 = \mu^{1/3} = 3^{1/3}\, r_H, \tag{14}$$

where $r_H = (\mu/3)^{1/3}$. Below this radius the smaller primary dominates the Hessian; above it the centrifugal and rescaled-solar terms do.

Solving (8) for β at a prescribed equilibrium position is elementary [1, 6]; what is shown here is that at the parity radius the solution collapses to a closed form in μ

Table 2 The closed form (17) against independent root-finding on $s(\beta) = 1$. Agreement is at machine precision for every mass ratio tested. $r_2/r_H = 3^{1/3} = 1.4422$ at parity by construction, independent of μ.

system	μ	β_{crit} (closed form)	β_{crit} (root-find)	$\lvert\Delta\rvert$	r_2 [nd]
Sun–Mercury	1.660×10^{-7}	0.010 961 524 792	0.010 961 524 792	3.1×10^{-16}	0.005 496
Sun–Earth	3.003×10^{-6}	0.028 646 456 169	0.028 646 456 169	2.1×10^{-16}	0.014 427
Sun–Jupiter	$9.538\,8 \times 10^{-4}$	0.187 186 695 655	0.187 186 695 655	2.8×10^{-16}	0.098 438
Earth–Moon	1.215×10^{-2}	0.406 934 946 280	0.406 934 946 280	5.0×10^{-16}	0.229 893

alone. Impose (14) on the balance (8). By the exact identity (2), $r_2 = \mu^{1/3}$ forces

$$r_1 = 1 - \mu^{1/3} \tag{15}$$

with no error term. Substituting, and using $x = (1-\mu) - r_2$ and $\mu/r_2^2 = \mu^{1/3}$,

$$\underbrace{(1-\mu) - \mu^{1/3}}_{x} = \frac{(1-\beta)(1-\mu)}{\left(1-\mu^{1/3}\right)^2} - \mu^{1/3}. \tag{16}$$

The $\mu^{1/3}$ terms cancel identically, leaving $(1-\mu) = (1-\beta)(1-\mu)\left(1-\mu^{1/3}\right)^{-2}$ and hence $1-\beta = \left(1-\mu^{1/3}\right)^2$. Therefore

$$\boxed{\beta_{\text{crit}} = 1 - \left(1-\mu^{1/3}\right)^2 = 2\mu^{1/3} - \mu^{2/3}} \tag{17}$$

This is exact for every μ; the cancellation is algebraic and involves no expansion in μ. To leading order $\beta_{\text{crit}} \simeq 2\mu^{1/3}$.

The same substitution gives the linear structure at parity in closed form,

$$c_2^{\text{parity}} = 1 + \frac{1-\mu}{1-\mu^{1/3}}, \tag{18}$$

which for Sun–Earth is 2.014635, the value quoted in Section 3.

4.2 Verification

We evaluate (17) against independent Brent root-finding on $s(\beta) - 1$, where s is computed from the numerically solved equilibrium (8). Table 2 reports both across five decades of mass ratio. Over a 61-point logarithmic sweep of $\mu \in [10^{-7}, 10^{-2}]$ the two never differ by more than 1.9×10^{-15}, i.e. a few units in the last place; at Sun–Earth the discrepancy is 2.1×10^{-16}. The two computations share no code path beyond the balance itself.

For Sun–Earth the threshold corresponds to a standoff $r_2 = 0.014\,427\,\text{nd} = 2\,158\,294\,\text{km} = 1.4422\,r_H$. For reference, the classical L_1 already sits at $r_2 = 0.9967\,r_H$, essentially on the Hill sphere, so the Hill-sphere exit criterion $r_2 = r_H$ is reached almost immediately, at $\beta = 2.981\,4 \times 10^{-4}$, and is not a useful discriminant.

4.3 Parity is one level of a hierarchy, and the distinguished one

The level $s = 1$ is a choice, and a reader is entitled to ask what privileges it. We answer by generalising. Impose instead $s = \kappa$ for arbitrary $\kappa > 0$, so that

$$r_2(\kappa) = \left(\frac{\mu}{\kappa}\right)^{1/3} = \left(\frac{3}{\kappa}\right)^{1/3} r_H, \tag{19}$$

and repeat the substitution of Section 4. Because $r_1 + r_2 = 1$ is exact, $r_1 = 1 - r_2(\kappa)$ with no error term, and the balance (8) gives a closed form for every κ,

$$\beta(\kappa) = 1 - \frac{(1 - r_2)^2}{1 - \mu}\Big[(1 - \mu) + \underbrace{\mu^{1/3}\kappa^{-1/3}(\kappa - 1)}_{\Delta(\kappa)}\Big]. \tag{20}$$

The bracketed correction $\Delta(\kappa) = -r_2 + \mu/r_2^2$ is the residue of the smaller primary's direct term after the standoff has been subtracted, and

$$\Delta(\kappa) = 0 \qquad \Longleftrightarrow \qquad \kappa = 1. \tag{21}$$

By (21), at $\kappa = 1$ and only there $\mu/r_2^2 = \mu^{1/3} = r_2$ identically: the tidal acceleration and the standoff cancel in the balance, (20) collapses to $1 - \beta = r_1^2$, and the threshold reduces to the pure square (17). Every other level leaves an explicit κ-dependent residue. *Tidal parity is therefore the unique level at which the smaller primary drops out of the on-axis balance identically*, which is a structural property of the balance rather than a preference about units — the objection we raised against ourselves at the start of Section 5.

Table 3 evaluates (20) across the hierarchy, and shows that the two levels this paper has already used are members of it. The classical L_1 is $\kappa = 3.0303$; the Hill-sphere exit criterion dismissed above is exactly $\kappa = 3$, since $s = 3 \Leftrightarrow r_2 = r_H$ by (19). What looked like two unrelated markers — one useful, one not — is one family sampled at two levels, with parity the distinguished member between them and the sail sweeping continuously through all of them.

4.4 An operational reading: what the saddle does to a mission

A level crossing says nothing by itself about whether a spacecraft notices. The quantity that does is the e-folding time of the residual instability,

$$\tau_u = \frac{1}{\lambda_u}, \qquad N_{\text{efold}} = \lambda_u T_{\text{mission}}, \tag{22}$$

with λ_u from (12) and time in units of $1/n$, one year divided by 2π, or 58.132 4 d for Sun–Earth. At $\beta = 0$ (22) returns $\tau_u = 22.95$ d, which is the familiar e-folding time of the Sun–Earth L_1 saddle; we did not fit it, and its recovery is a check on (12).

Table 3 The tidal-strength hierarchy $s = \kappa$ for Sun–Earth, evaluated from the closed form (20). $r_2/r_H = (3/\kappa)^{1/3}$ exactly, independent of μ. The last column is the e-folding time (22) of the residual saddle. Both markers used earlier in this paper appear as members: $\kappa = 3.0303$ is the classical L_1 and $\kappa = 3$ is the Hill-sphere exit.

κ	β	r_2 [nd]	r_2/r_H	standoff [km]	τ_u [d]
3.030 3	0.000 000	0.009 970	0.996 7	1 491 472	23.0
3	0.000 298	0.010 003	1.000 0	1 496 477	23.1
2	0.011 581	0.011 451	1.144 7	1 713 039	28.0
1	0.028 646	0.014 427	1.442 2	2 158 294	38.6
0.5	0.044 785	0.018 177	1.817 1	2 719 280	52.9
0.1	0.087 462	0.031 083	3.107 2	4 649 903	109.7
0.01	0.187 161	0.066 966	6.694 3	10 017 911	326.5

Table 4 Lightness number at which the residual saddle yields exactly one e-fold of departure over the stated horizon, Sun–Earth, $\alpha = 0$, obtained by root-finding on $\lambda_u(\beta)T = 1$. For comparison, tidal parity is $\beta = 0.028\,646$ with $\tau_u = 38.6$ d.

horizon	T [d]	$\lambda_u^\star$ [nd]	β	s
30 d	30	1.937 75	0.015 441	1.722 3
90 d	90	0.645 92	0.074 652	0.154 1
6 months	183	0.317 66	0.127 015	0.033 5
1 year	365	0.159 27	0.201 200	0.007 9
2 years	731	0.079 52	0.311 638	0.001 9

Inverting $N_{\text{efold}} = 1$ for β gives the lightness number at which the saddle can no longer produce even one e-fold of departure over a stated mission horizon. Table 4 reports it.

Two things follow, and they pull in opposite directions. Tidal parity sits between the 30 d and 90 d horizons: at β_{crit} the saddle still turns over in 38.6 d, so a spacecraft there is very far from free of it. Operational irrelevance over a realistic mission is a much stronger demand — $\beta = 0.127$ for six months, $\beta = 0.201$ for a year — which is a factor of 20 to 33 beyond the best sail yet flown (Section 8). The exact threshold and the operational one answer different questions and should not be conflated: (17) locates where the smaller primary stops dominating the Hessian, while Table 4 locates where it stops mattering to a mission. The first is exact and μ-independent in form; the second is a numerical root of a transcendental function and depends on the horizon one chooses. We report both because the first is the sharper statement and the second is the more useful one.

5 The frequency ratio: a universal bound on c_2

The threshold (17) is a level crossing of a smooth monotone function. Nothing bifurcates there, and the choice of the level $s = 1$ is partly a statement about the

non-dimensionalisation. The standard route to promoting such a marker into a dynamical event is a commensurability of the linear frequencies. This section searches for one and reports that none exists — together with an exact extremum that does.

5.1 The bound and its extremum

From (12), the ratio of the out-of-plane to in-plane frequency depends on c_2 alone,

$$\frac{\nu^2}{\omega^2} = \frac{2c_2}{D-(c_2-2)}, \qquad D = \sqrt{c_2(9c_2-8)}. \tag{23}$$

The two frequencies in (12) are standard — they appear in this form in [25, 26, 28, 29]. Their difference, the detuning $\omega - \nu$, has been studied as a function of μ at the classical points [29, 30], and the bifurcation thresholds to halo orbits have been analysed in the same framework with radiation pressure included [31]. To our knowledge the ratio ν/ω, its sharp lower bound and the point at which it is attained have not been stated. That is what follows.

Differentiating (23), the stationarity condition reduces to $D = 2c_2$, i.e. $9c_2^2 - 8c_2 = 4c_2^2$, giving

$$\boxed{c_2^\star = \tfrac{8}{5}} \tag{24}$$

and there, from (12),

$$\lambda_u = \sqrt{\tfrac{7}{5}}, \qquad \nu = \sqrt{\tfrac{8}{5}}, \qquad \omega = \sqrt{\tfrac{9}{5}} \qquad \Longrightarrow \qquad \lambda_u^2 : \nu^2 : \omega^2 = 7 : 8 : 9, \tag{25}$$

$$\frac{\nu}{\omega}\Big|_{c_2^\star} = \sqrt{\tfrac{8}{9}} = \frac{2\sqrt{2}}{3} = 0.942809041582\ldots \tag{26}$$

Over the whole physically admissible range $c_2 > 1$ the ratio is confined to

$$\frac{\nu}{\omega} \in \Big[\tfrac{2\sqrt{2}}{3},\, 1\Big), \tag{27}$$

a band 5.72 % wide, approaching unity in the hovering limit $c_2 \to 1$ and again as $c_2 \to \infty$. Numerically, a 4×10^5-point scan over $c_2 \in [1, 4.2]$ returns a minimum value 0.942809041582, agreeing with (26) to 1.1×10^{-16}, i.e. to one unit in the last place. The scan locates the minimiser only to its grid resolution of $\frac{1}{2} \times 8.0 \times 10^{-6}$, which is consistent with $c_2^\star = 8/5$ but does not independently confirm it to more digits than that; the value is far more accurate than the location because (23) is stationary, and therefore quadratically flat, at $c_2^\star$. The exact statement rests on (24), not on the scan. Note that $c_2^\star$, the ratios (25) and the bound (26) contain no reference to μ: they are properties of the collinear linearisation itself, shared by every three-body system.

The narrowness of (27) has been observed qualitatively. Ceccaroni *et al.* [27, 29], sweeping all three collinear points over the full range $\mu \in (0, \frac{1}{2}]$, note that the centre-manifold dynamics is "characterized by almost equal values of the frequencies for all mass ratios". Equations (27) and (26) make that observation exact and supply the constant it is missing.

The observation is not merely descriptive: it is load-bearing. Celletti, Lhotka and Pucacco [32] build their normal form for the collinear points of the elliptic problem on exactly this near-equality, assuming the two elliptic frequencies equal and displacing their difference into a first-order term through a detuning parameter $\delta \equiv \omega_y - \omega_z$. Read in that setting, (27) bounds the detuning: $\delta > 0$ strictly for $c_2 > 1$, so the 1:1 resonance is never exactly attained, and the relative detuning $1 - \nu/\omega$ can never exceed 5.72 % at any collinear point of any three-body system. The near-equality such schemes rely on is therefore a structural property with an explicit bound, not an empirical convenience.

5.2 No low-order resonance is attainable

We tested fourteen low-order rationals — 1:2, 2:3, 3:4, 4:5, 5:6, 8:9, 1:1, 9:8, 6:5, 5:4, 4:3, 3:2, 5:3, 2:1 — against the band (27). *None* lies inside it. Since $\nu < \omega$ strictly for $c_2 > 1$, even the 1:1 commensurability is approached only asymptotically, as the equilibrium degenerates into the hovering point. In particular the non-resonance condition of the Lyapunov centre theorem — that neither frequency be an integer multiple of the other, which in the classical problem is known to fail at most on a countable set of mass ratios [26] — holds at every collinear equilibrium, sail or classical, since $1 < \omega/\nu \leq 3/(2\sqrt{2})$.

A spot check of fourteen rationals is weaker than the band deserves, because (27) admits an exact statement. The band is a left-closed interval with right endpoint 1, so the only rationals it can contain with denominator q are those nearest unity, and the largest rational below unity at denominator q is $(q-1)/q$. Hence a commensurability p:q lies in (27) only if

$$\frac{q-1}{q} \;\geq\; \frac{2\sqrt{2}}{3} \qquad \Longleftrightarrow \qquad q \;\geq\; \frac{1}{1 - 2\sqrt{2}/3} = 17.485\ldots, \tag{28}$$

that is, only if $q \geq 18$. *The band therefore contains no commensurability of denominator below* 18 *at all*, and the lowest-order one inside it is $17{:}18 = 0.9444\ldots$, of order $p+q = 35$. The fourteen rationals above have denominators at most 9 and are excluded by (28) without needing to be tested individually.

The consequence is that no commensurability of any order a perturbation theory would ordinarily retain underwrites tidal parity, or arises anywhere else in the face-on solar-sail CR3BP. Equation (17) must therefore be presented as an exact *scale marker* with a clean geometric reading, not as a dynamical transition. We regard this negative as a result rather than an omission: it is the check a reader is entitled to demand, and it forecloses an over-claim. We stress that the band is not resonance-free in the strict sense — (28) shows it is dense with rationals of denominator 18 and above — only that every one of them is of order 35 or higher.

Two caveats. First, (27) constrains the *linear* frequencies only. Halo families bifurcate from planar Lyapunov families at a commensurability of the *nonlinear* frequencies, reached at finite amplitude; the classical L_1 has $\nu/\omega = 0.9659$ and halo orbits exist there regardless. Nothing here constrains halo existence. Second, $c_2^\star$ is a stationary point, not a transition: the dynamics change character nowhere in c_2. Its value is

that a stationary point is intrinsic — it survives any smooth reparametrisation and any choice of units — whereas a level crossing at $s = 1$ does not.

5.3 What the sail contributes

It would be natural to suppose $c_2^\star = 8/5$ inaccessible without continuous thrust, on the grounds that the classical collinear points have $c_2 \geq 4$. That is true only of L_1. Computing c_2 at all three classical collinear points over $\mu \in (0, \frac{1}{2}]$ gives

$$c_2(L_1) \in [4.042,\, 8.000], \qquad c_2(L_2) \in [1.570,\, 3.959], \qquad c_2(L_3) \in [1.000,\, 1.570], \quad (29)$$

so the classical problem covers $c_2 < 4$ freely at L_2 and L_3, and it *does* attain $c_2^\star$: at L_2 with $\mu = 0.480187660$, where ν/ω equals (26) to twelve digits. L_3 at $\mu = \frac{1}{2}$ reaches $c_2 = 1.569787$ and misses the bound by only 3.07×10^{-5} — close enough that the near-coincidence is worth recording, since L_3 occupies precisely the interval in which the extremum lies.

The sail's contribution is therefore *tunability*, not exclusivity, and (10) is the compact way to say it: at fixed μ a sail sweeps c_2 continuously through $(1, c_2^{\text{classical}}]$, whereas classically c_2 is fixed once the system and the point are chosen. Sun–Earth classically offers only $c_2 = 4.060819$ at L_1, 3.940764 at L_2 and 1.000003 at L_3; none is at the bound, and a sail at $\beta = 0.040932$ places that system exactly on it — a factor 1.4289 beyond tidal parity, at $s = 0.5897$. Figure 3 collects all of this.

6 Halo families across the flown sail band

The band $\beta \in [0.001, 0.05]$ is where a sail both matters dynamically and still inhabits a genuine three-body structure: below it the sail is irrelevant, and above tidal parity the collinear structure has lost its meaning. We therefore walk the halo family at twelve values of β across that band. The classical family is the one of Breakwell and Brown [33] and Howell [34], and continuation of libration-point families follows Doedel *et al.* [35]. The evolution of this family with β in the same face-on sail problem was studied by Verrier, Waters and Sieber [13], who report that a branch point at $\beta \approx 0.0387$ splits the L_1 halo family; that value lies inside the band walked here, and we compare against it at the end of this section.

Two methodological points are load-bearing. First, all lengths are expressed in units of the local scale $\gamma = |(1-\mu) - x_{\text{eq}}|$, which doubles across the band (0.0101 at $\beta = 0.001$ to 0.0196 at $\beta = 0.05$). Absolute step sizes and amplitude bounds therefore mean different things at different β; fixed ones admit far-field orbits, and a seed amplitude of $A_z = 0.02$ — reasonable for Earth–Moon — is roughly 2γ for Sun–Earth, larger than the entire distance from the equilibrium to the smaller primary.

Second, the differential corrector solves for $[x_0,\, \dot{y}_0,\, T/2]$ subject to $[\dot{x}_f,\, \dot{z}_f,\, y_f] = 0$; z_0 is not a free variable and A_z is not a constraint. Stepping A_z and re-solving therefore fails at folds in A_z, where the branch turns and no solution exists at the requested amplitude. We use pseudo-arclength continuation, appending the arclength condition and treating the continuation parameter as an unknown, so that folds are traversed rather than tripped over. Branch identity is additionally enforced across β: each β is

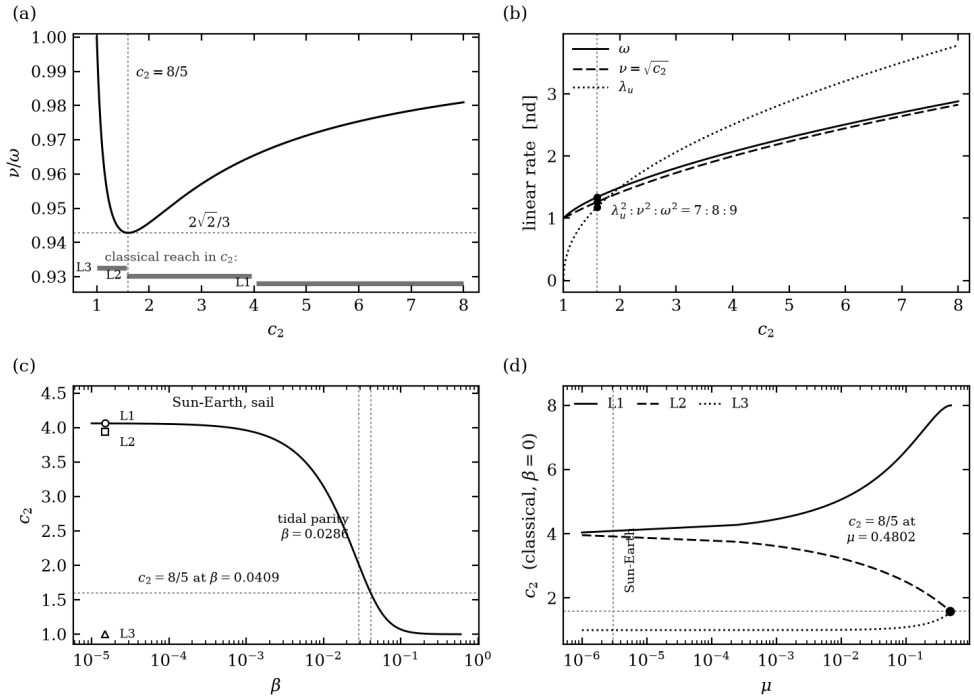


Fig. 3 The frequency ratio at collinear equilibria. **(a)** ν/ω against c_2, with the exact minimum $2\sqrt{2}/3$ at $c_2 = 8/5$ and, in the reserved strip below, the ranges of c_2 reached by the three classical collinear points over $\mu \in (0, \frac{1}{2}]$; the vertical placement of those bars is a layout choice and carries no value. **(b)** The three linear rates, meeting the ratio $7 : 8 : 9$ at $c_2^\star$. **(c)** The sail's tuning curve for Sun–Earth: $c_2(\beta)$ sweeps continuously from the classical value down to unity, passing tidal parity and then $c_2^\star$. Open markers give the three classical Sun–Earth values, none of which is at the bound. **(d)** Classical c_2 against μ for all three points; $c_2^\star$ is attained at L_2 for $\mu = 0.4802$.

seeded from its predecessor's converged state with z_0 rescaled by $\gamma_{\text{new}}/\gamma_{\text{old}}$, and two guards verify the result — the sign of the z-extremum asymmetry

$$\Delta_z = \frac{|z_0| - |z(T/2)|}{|z_0| + |z(T/2)|} \tag{30}$$

must match the reference β, and the family must lie sunward of the equilibrium. Δ_z is $O(0.1)$ for a genuine halo over most of the band and vanishes identically on the vertical-Lyapunov branch, which makes it an effective discriminator. It does weaken as the band is traversed: the smallest $|\Delta_z|$ in the family falls from 0.109 at $\beta = 0.001$ to 0.0898 at $\beta = 0.040$ and 0.0125 at $\beta = 0.050$, so at the upper end it separates the branches by an order of magnitude rather than two. The guard is not decorative. Re-walking $\beta = 0.040$ with the cross-β seeding disabled — so that the amplitude scan is

Table 5 How the continued L_1 halo family ends, walked to termination on a fine grid in β (budget 450 members, chained seeding). *Bound*: the walk reached the amplitude bound $A_z = \gamma$. *Planar*: it turned back to $A_z = 0$. Folds counts turning points in A_z. Reproduced by `python main.py atlas_fine`.

β	members	max A_z/γ	folds	end
0.032	298	0.996	2	bound
0.034	305	0.990	2	bound
0.036	308	0.990	2	bound
0.038	313	0.992	2	bound
0.039	81	0.784	2	planar
0.0395	56	0.781	2	planar
0.040	40	0.776	1	planar
0.042	32	0.760	1	planar
0.045	57	0.739	1	planar

restarted independently at that β, as an earlier version of this pipeline did — lands on a branch that runs Earthward instead of sunward and is rejected by the far-field guard with x_0 reaching the smaller primary, so no family is returned at all. Seeded instead from its converged predecessor at $\beta = 0.032$, the same β yields 40 members with $\Delta_z \in [0.090, 0.161]$, every one of them sunward of the equilibrium. One of the twelve atlas curves is therefore a different family unless branch identity is enforced across β.

Figure 4 reports the resulting atlas. The Jacobi constant is computed from (6); because the potential (5) is itself β-dependent, raw C_{sail} is not comparable across β, and we plot instead the depth below the local equilibrium, $C_{\mathrm{sail}} - C_{\mathrm{sail}}(x_{\mathrm{eq}})$, against A_z/γ.

Comparison with Verrier, Waters and Sieber.

The atlas walks stop after 70 members, which characterises each family but does not show where it ends. To locate the end, we re-walk nine values of β between 0.032 and 0.045 with a budget of 450 members, enough for every walk to terminate on a bound, and classify each family by how it terminates (Table 5). Up to $\beta = 0.038$ the family runs out to the amplitude bound $A_z = \gamma$ after about 300 members and two folds. From $\beta = 0.039$ onward it turns back and returns to $A_z = 0$, that is, to the planar Lyapunov family, after at most 81 members. The change therefore lies in $\beta \in (0.038, 0.039]$, an interval that contains the branch point $\beta \approx 0.0387$ at which Verrier *et al.* [13] find the L_1 halo family split. The two calculations use different continuation schemes and different diagnostics, so we read the agreement as an independent check of their value, here to within 10^{-3} in β. We do not resolve the branch point itself, only the change in where the continued family ends; the $\beta = 0.040$ walk of the main atlas, which also returns to $A_z = 0$ after 40 members, lies on the far side of it.

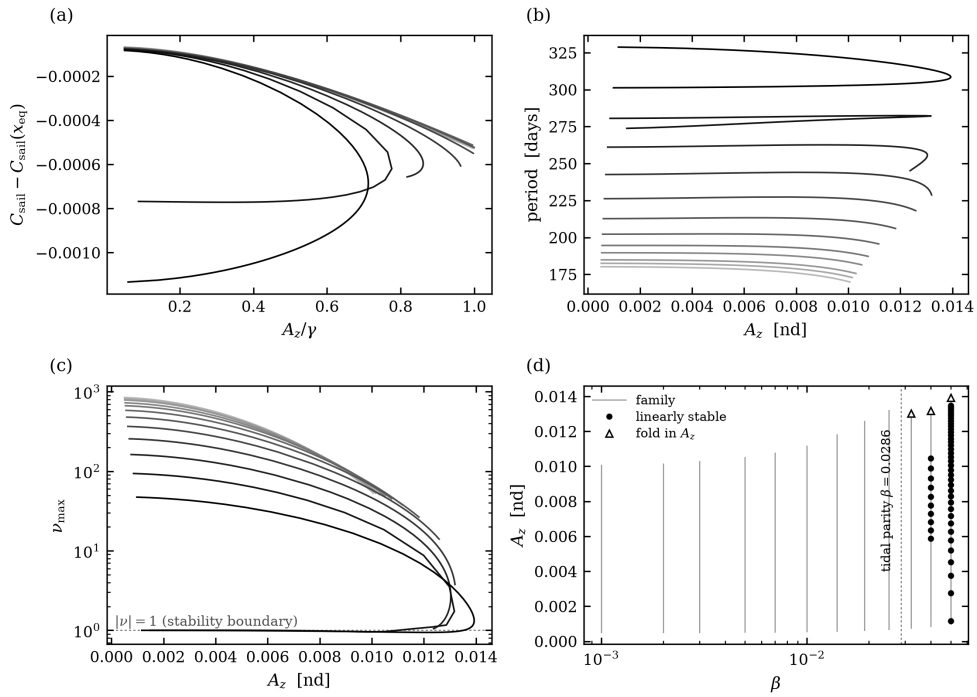


Fig. 4 Halo families across $\beta \in [0.001, 0.05]$, Sun–Earth, $\alpha = 0$, walked by pseudo-arclength continuation with branch identity enforced across β. **(a)** Family depth below the local equilibrium in the sail potential, against amplitude scaled by the local length γ. **(b)** Period. **(c)** Stability index, with the $|\nu| = 1$ boundary. **(d)** The (β, A_z) plane: family extent, folds, and linearly stable segments, with tidal parity marked.

7 Control authority of a face-on sail

The dynamics above are open-loop. Since equilibria in this region are unstable, it is natural to ask what a sail can do about it, and here the face-on configuration turns out to be singular.

A sail has two control inputs, the attitude angles, and its thrust direction is rigidly coupled to its magnitude through (3). Linearising in (α, δ) about a nominal (α_0, δ_0) gives a 6×2 control Jacobian $B_{\rm sail}$ whose non-trivial rows are $\partial \boldsymbol{a}/\partial\alpha$ and $\partial \boldsymbol{a}/\partial\delta$. At $\alpha_0 = 0$ exactly,

$$\frac{\partial \boldsymbol{a}}{\partial \alpha} = \beta \frac{1-\mu}{r_1^2}\big(\cos\delta_0\, \hat{\boldsymbol{p}} + \sin\delta_0\, \hat{\boldsymbol{q}}\big), \qquad \frac{\partial \boldsymbol{a}}{\partial \delta} = \boldsymbol{0}. \tag{31}$$

The clock angle has *no* first-order authority when the sail is face-on: it only rotates a normal already parallel to $\hat{\boldsymbol{r}}$. The single available direction is therefore fixed by

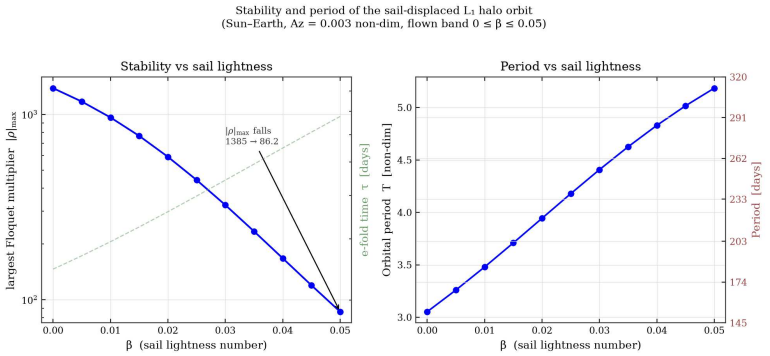


Fig. 5 Largest Floquet multiplier (left) and period (right) of the L_1 halo orbit with $A_z = 0.003$ across the flown band $0 \le \beta \le 0.05$; every member is checked to be a halo rather than a vertical Lyapunov orbit. The decline is not sail stabilisation of a saddle: the standoff grows, the smaller primary's tidal term weakens, and the orbit moves away from the saddle it began near.

the constant δ_0, and it is purely transverse, since $\boldsymbol{a} \cdot \hat{\boldsymbol{r}} = \beta(1-\mu)r_1^{-2}\cos^3\alpha$ and $\mathrm{d}(\cos^3\alpha)/\mathrm{d}\alpha \to 0$ as $\alpha \to 0$.

Rank of B is not the relevant test, because Coriolis coupling can carry a transverse input into the radial direction. Applying the Kalman rank condition to the linearised system at the $\beta = 0.05$ equilibrium ($c_2 = 1.409194$):

control model	Kalman rank	verdict
unconstrained three-axis thruster (6×3)	6/6	controllable
sail, $\alpha_0 = 0$, $\delta_0 = 0$	4/6	**uncontrollable**
sail, $\alpha_0 = 0$, $\delta_0 = \pi/2$	2/6	**uncontrollable**
sail, $\alpha_0 = 0$, $\delta_0 = \pi/4$	6/6	controllable (one input)
sail, $\alpha_0 \ge 0.5°$	6/6	controllable

The in-plane four-state block *is* controllable by a single transverse input (rank 4/4) — Coriolis does the work — so the absent radial authority is not by itself fatal. Because $\partial\boldsymbol{a}/\partial\delta = \boldsymbol{0}$, a face-on sail has a single input, whose direction is fixed by δ_0, and its controllability depends on that direction. Purely in-plane ($\delta_0 = 0$), it cannot reach the vertical mode, which decouples at linear order; purely vertical ($\delta_0 = \pi/2$), it cannot reach the in-plane pair. For any other δ_0 the single input excites both blocks, and since their spectra $\{\pm\lambda_u, \pm\mathrm{i}\omega\}$ and $\{\pm\mathrm{i}\nu\}$ are disjoint whenever $\nu \neq \omega$ — which (27) guarantees at every collinear equilibrium — the Popov–Belevitch–Hautus test gives full rank. The face-on nominal is therefore not uncontrollable; what it loses is one of its two inputs:

$$\alpha_0 = 0 \text{ is a singular nominal for two-input attitude control.} \tag{32}$$

In the cone/clock parametrisation this is partly a coordinate effect, noted by Huang *et al.* [19], who adopt pitch and azimuth angles for that reason; physically, the first-order authority of a face-on sail is confined to one transverse direction chosen in advance. Any non-zero cone angle restores the second input; 0.5° suffices formally, though the

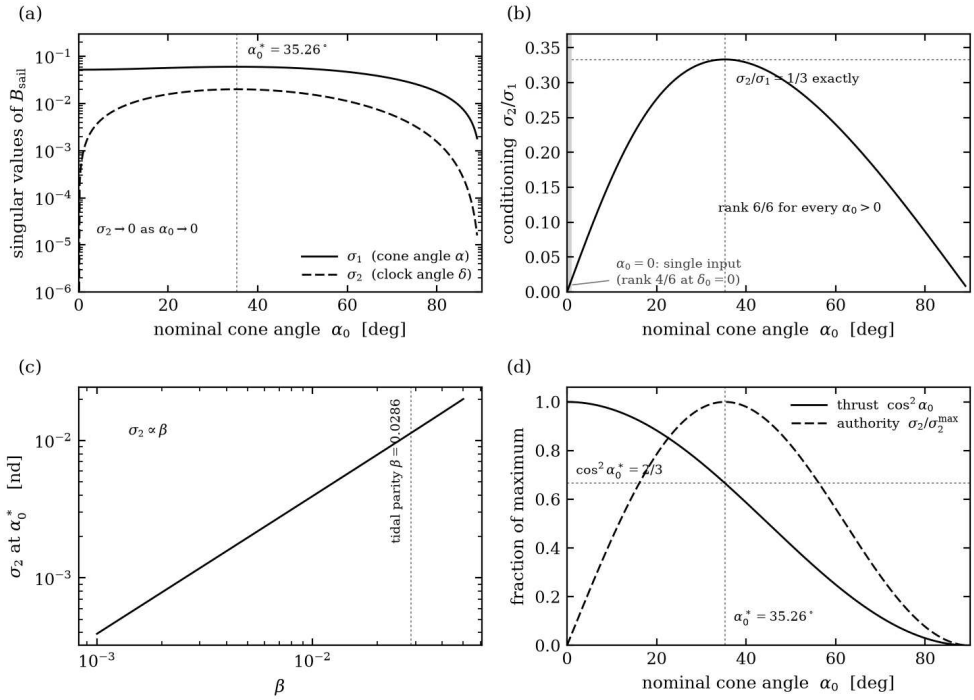


Fig. 6 Control authority of a solar sail at the artificial equilibrium, $\beta = 0.05$. **(a)** Singular values of B_{sail} against nominal cone angle; $\sigma_2 \to 0$ as $\alpha_0 \to 0$. **(b)** Conditioning, maximal at $\alpha_0^\star$ with the exact value 1/3; the shaded strip at the origin marks the single-input nominal. **(c)** Out-of-plane authority scales linearly with β. **(d)** The design trade, both curves dimensionless: thrust $\cos^2 \alpha_0$ against normalised authority.

second singular value of B_{sail} there is 4.5×10^{-4} against 5.2×10^{-2} for the first, a 115:1 conditioning penalty, so usable two-input authority requires a few degrees.

Authority is maximised at

$$\alpha_0^\star = \arctan\!\left(1/\sqrt{2}\right) = 35.264^\circ, \qquad \frac{\sigma_2}{\sigma_1} = \frac{1}{3}, \qquad \cos^2 \alpha_0^\star = \frac{2}{3}, \tag{33}$$

all exact and independent of β. This angle is the classical optimal sail cone angle for maximum transverse thrust [6, §2.6]; recovering it from the control Jacobian is a benchmark check on (31), not a new result. What is new is that the same angle maximises out-of-plane control authority, with σ_2/σ_1 exactly 1/3 there, and that the second singular value of B_{sail} vanishes identically at $\alpha_0 = 0$. Figure 6 shows the trade: thrust falls as $\cos^2 \alpha_0$ while authority rises from zero, and $\alpha_0^\star$ is where the second is maximal.

Table 6 Lightness number of every solar sail flown or funded to flight hardware, reduced from primary specifications. β_{ideal} is the perfect-reflector limit; β_{eff} applies the optical efficiency $\eta = 1.12/1.78 = 0.629$, the ratio of the IKAROS thrust estimated from orbit determination (1.12 mN [41]) to the ideal flat-sail value $2PA = 1.78$ mN at 1 au. IKAROS is the only entry whose lightness number follows from an in-flight thrust estimate rather than from area and mass; the heliocentric distance of that estimate is not reported, so its β and η are approximate. Solar Cruiser has no published mass; its β_{ideal} is reduced instead from the published characteristic acceleration $\geq 0.12\,\mathrm{mm\,s^{-2}}$, and is therefore a lower bound rather than a value obtainable from the area column.

mission	area [m^2]	mass [kg]	β_{ideal}	β_{eff}	status
IKAROS [36, 37]	196	307	0.000 98	0.000 62	flown 2010, in-flight estimate
LightSail-2 [38]	32	5	0.009 80	0.006 17	flown 2019
NEA Scout [39]	86	14	0.009 41	0.005 92	sail not deployed, lost 2022
ACS3 [40]	80	16	0.007 66	0.004 82	flown 2024
Solar Cruiser	1653	—	0.020 24	—	cancelled 2022

8 Where the threshold sits against flown hardware

The threshold (17) is only interesting if it is within reach. We therefore reduce β from primary mission specifications rather than quoting secondary values, using $\beta = \sigma^*/\sigma$ with the critical sail loading $\sigma^* = 2P/g_\odot$. Evaluated from CODATA and IAU constants, $\sigma^* = 1.531\,1\,\mathrm{g\,m^{-2}}$, reproducing McInnes' 1.53 [6] to the three figures he quotes, which validates the chain.

No sail flown and deployed reaches $\beta = 0.006\,2$ — the best is LightSail-2 at $\beta = 0.006\,17$ — and the only value based on an in-flight thrust estimate is IKAROS at $\beta = 0.000\,62$. Against $\beta_{\mathrm{crit}} = 0.028\,646$:

reference	β	shortfall
best flown, perfect-reflector limit (LightSail-2)	0.009 799	2.9×
best flown, realistic (LightSail-2)	0.006 167	4.6×
only in-flight estimate (IKAROS)	0.000 615	47×
most ambitious funded design (Solar Cruiser, cancelled)	0.020 236	1.4×

Tidal parity is therefore a factor of 4.6 beyond the best sail flown and deployed — 2.9 if that sail is credited with a perfect reflector — and a factor of 1.4 beyond the most ambitious design funded to flight hardware. The defensible statement is that it lies at the edge of *near-term* rather than current capability. We note explicitly that a claim of the form "$\beta \sim 0.01$–0.05 is current technology", which appears informally, is not supported by any flown mission.

A consequence worth stating: at the best flown $\beta \approx 0.006$ the saddle strength is $s \approx 2.5$, so for every sail ever flown the collinear structure is fully intact and smaller-primary-dominated. The dissolution characterised here is a prediction about a regime not yet reached, not an account of observed behaviour.

9 Limitations

1. **Face-on only.** Everything except Section 7 assumes $\alpha = 0$. For $\alpha \neq 0$ the force is non-conservative, no Jacobi integral exists, and the effective-potential analysis used throughout fails. The steered case is open and is the natural sequel.

2. **Ideal specular reflector.** Membrane billow, finite slew rate, self-shadowing, and wavelength-dependent optics are not modelled. Dachwald *et al.* [12] argue persuasively that non-ideal optics matter more than order-of-magnitude estimates suggest; the IKAROS efficiency $\eta = 0.629$ in Table 6 is a single-mission proxy, not a general correction. Generalised-sail models [9, 42] are the natural setting for that extension, and the elliptic problem, in which the equilibria themselves become periodic, has been treated for sails in [10, 16].
3. **No bifurcation is claimed.** $s > 0$ for all finite r_2, so the saddle persists; $c_2^\star$ is a stationary point of a smooth function. Both thresholds are exact structural landmarks, and the resonance search of Section 5 is what licenses that restraint.
4. **Derived hardware figures.** Every β in Table 6 except IKAROS' is reduced by us from published area and mass, not quoted by the mission teams. Where a team publishes its own lightness number, prefer it.
5. **Linear controllability only.** Section 7 is a statement about the linearisation at the equilibrium. Nonlinear or higher-order control strategies at $\alpha_0 = 0$ are not excluded; only first-order authority is.

10 Conclusions

A face-on solar sail rescales solar gravity rather than perturbing the collinear point, so the collinear structure does not shift with β — it decays. We have characterised that decay through the saddle strength $s = \mu/r_2^3$, which falls four decades between $\beta = 0$ and $\beta = 0.5$, and obtained two exact results.

The tidal-parity threshold admits the closed form $\beta_{\text{crit}} = 2\mu^{1/3} - \mu^{2/3}$, exact for every mass ratio and verified to machine precision across five decades of μ. For Sun–Earth it is 0.0286, corresponding to a standoff of $3^{1/3} r_H$. The scale $\mu^{1/3}$ is not itself new; the exact sail parameter required to reach it is. Nor is the level $s = 1$ arbitrary: the generalisation $s = \kappa$ admits a closed form for every κ, but only at $\kappa = 1$ does the smaller primary's direct term cancel out of the balance identically, and both the classical L_1 ($\kappa = 3.0303$) and the Hill-sphere exit ($\kappa = 3$) are members of the same family. Read through the e-folding time, parity is a 38.6 d saddle; making the saddle operationally irrelevant over six months demands $\beta = 0.127$, twenty times the best sail flown.

The parameter A of the collinear linearisation is exactly Richardson's second Legendre coefficient c_2, and a sail's effect is to detune it continuously. The frequency ratio at any collinear equilibrium is confined to $\nu/\omega \in [2\sqrt{2}/3, 1)$ and attains its bound at $c_2 = 8/5$, where the linear rates stand in the ratio $7 : 8 : 9$. Both are independent of μ. The near-equality of the two frequencies has been noted before [29]; the bound and its extremum make it exact. No low-order rational lies in the band, so no commensurability underwrites either threshold, and we present them as scale markers rather than transitions. The sail's role is to tune c_2 within a given system, reaching values — including the bound, at $\beta = 0.0409$ for Sun–Earth — that that system's classical collinear points do not offer.

Re-walking the halo family to termination on a fine grid in β places the change in where it ends in (0.038, 0.039], bracketing the branch point reported by Verrier *et al.* at $\beta \approx 0.0387$.

Finally, the face-on nominal is singular in the attitude angles: the clock angle has no first-order authority, so a face-on sail is a single-input system, controllable only when its tilt direction has both in-plane and vertical components, and a few degrees of cone angle are required to recover a well-conditioned second input. Authority peaks at the classical optimal cone angle $\arctan(1/\sqrt{2})$, where the conditioning is exactly 1/3.

Set against flown hardware, tidal parity is a factor 4.6 beyond the best deployed sail and 47 beyond the only lightness number estimated in flight. It is a near-term design boundary, not a present one.

Supplementary information. The derivations companion (`companion.pdf`) gives the full algebra behind every closed-form result in this paper and is provided as Online Resource 1.

Acknowledgements. None.

Declarations

Funding. The author did not receive support from any organization for the submitted work.

Competing interests. The author has no relevant financial or non-financial interests to disclose.

Use of AI-assisted tools. The author used Claude as an assistant for editing manuscript text, for auditing the numerical claims of the manuscript against the code output, and for searching and checking references. The author conceived and directed the study, chose the models and parameters, ran all computations and interpreted the results, and reviewed and verified all AI-assisted text, including through the automated check of every number in the paper described below. The author takes full responsibility for the content of this manuscript.

Data and code availability. All numerical results, figures and the verification suite are reproducible from a single entry point. The complete source is public at https://github.com/Bishwaswarup/SOLAR_SAIL; the state corresponding to this version is tagged `researchsquare-v1` (preprint) and `cmda-v1` (journal submission). Every quantity quoted in this paper is regenerated by `python main.py` and written to a machine-generated results file; no value is hand-transcribed. `paper/verify_numbers.py` recomputes the numerical claims from the source modules and compares each against the literal typed here, failing if any has drifted; Tables 2, 3 and 4 are parsed cell by cell out of the manuscript source.

Author contributions. B.N. conceived the study, developed the software, performed the analysis and wrote the manuscript.

Ethics approval and consent to participate. Not applicable.

References

[1] McInnes, C.R., McDonald, A.J., Simmons, J.F.L., MacDonald, E.W.: Solar sail parking in restricted three-body systems. Journal of Guidance, Control, and Dynamics **17**(2), 399–406 (1994) https://doi.org/10.2514/3.21211

[2] Baoyin, H., McInnes, C.R.: Solar sail halo orbits at the Sun–Earth artificial L_1 point. Celestial Mechanics and Dynamical Astronomy **94**(2), 155–171 (2006) https://doi.org/10.1007/s10569-005-4626-3

[3] Waters, T.J., McInnes, C.R.: Periodic orbits above the ecliptic in the solar-sail restricted three-body problem. Journal of Guidance, Control, and Dynamics **30**(3), 687–693 (2007) https://doi.org/10.2514/1.26232

[4] Farrés, A., Jorba, À.: Periodic and quasi-periodic motions of a solar sail close to SL_1 in the Earth–Sun system. Celestial Mechanics and Dynamical Astronomy **107**(1–2), 233–253 (2010) https://doi.org/10.1007/s10569-010-9268-4

[5] Farrés, A., Jorba, À.: Station keeping strategies for a solar sail in the solar system. In: Advances in Astrodynamics and Space Applications. Springer, Cham (2016). https://doi.org/10.1007/978-3-319-27464-5_3

[6] McInnes, C.R.: Solar Sailing: Technology, Dynamics and Mission Applications. Springer, Chichester, UK (1999). https://doi.org/10.1007/978-1-4471-3992-8

[7] Simmons, J.F.L., McDonald, A.J.C., Brown, J.C.: The restricted 3-body problem with radiation pressure. Celestial Mechanics **35**(2), 145–187 (1985) https://doi.org/10.1007/BF01227667

[8] Morimoto, M.Y., Yamakawa, H., Uesugi, K.: Artificial equilibrium points in the low-thrust restricted three-body problem. Journal of Guidance, Control, and Dynamics **30**(5), 1563–1568 (2007) https://doi.org/10.2514/1.26771

[9] Aliasi, G., Mengali, G., Quarta, A.A.: Artificial equilibrium points for a generalized sail in the circular restricted three-body problem. Celestial Mechanics and Dynamical Astronomy **110**(4), 343–368 (2011) https://doi.org/10.1007/s10569-011-9366-y

[10] Aliasi, G., Mengali, G., Quarta, A.A.: Artificial equilibrium points for a generalized sail in the elliptic restricted three-body problem. Celestial Mechanics and Dynamical Astronomy **114**(1-2), 181–200 (2012) https://doi.org/10.1007/s10569-012-9425-z

[11] Mengali, G., Quarta, A.A., Circi, C., Dachwald, B.: Refined solar sail force model with mission application. Journal of Guidance, Control, and Dynamics **30**(2), 512–520 (2007) https://doi.org/10.2514/1.24779

[12] Dachwald, B., Macdonald, M., McInnes, C.R., Mengali, G., Quarta, A.A.: Solar sails are not ideal, and yes it matters. In: Advances in Solar Sailing. Springer, Berlin, Heidelberg (2013). https://doi.org/10.1007/978-3-642-34907-2_55

[13] Verrier, P., Waters, T., Sieber, J.: Evolution of the $\mathcal{L}_1$ halo family in the radial solar sail circular restricted three-body problem. Celestial Mechanics and Dynamical Astronomy **120**(4), 373–400 (2014) https://doi.org/10.1007/s10569-014-9575-2

[14] Bookless, J., McInnes, C.: Dynamics and control of displaced periodic orbits using solar-sail propulsion. Journal of Guidance, Control, and Dynamics **29**(3), 527–537 (2006) https://doi.org/10.2514/1.15655

[15] Bookless, J., McInnes, C.: Control of Lagrange point orbits using solar sail propulsion. Acta Astronautica **62**(2-3), 159–176 (2008) https://doi.org/10.1016/j.actaastro.2006.12.051

[16] Biggs, J.D., McInnes, C.R., Waters, T.: Control of solar sail periodic orbits in the elliptic three-body problem. Journal of Guidance, Control, and Dynamics **32**(1), 318–320 (2009) https://doi.org/10.2514/1.38362

[17] Farrés, A., Jorba, À.: Solar sail surfing along families of equilibrium points. Acta Astronautica **63**(1-4), 249–257 (2008) https://doi.org/10.1016/j.actaastro.2007.12.021

[18] Farrés, A., Jorba, À.: Station keeping of a solar sail around a halo orbit. Acta Astronautica **94**(1), 527–539 (2014) https://doi.org/10.1016/j.actaastro.2012.07.002

[19] Huang, J., Biggs, J.D., Cui, N.: Families of halo orbits in the elliptic restricted three-body problem for a solar sail with reflectivity control devices. Advances in Space Research **65**(3), 1070–1082 (2020) https://doi.org/10.1016/j.asr.2019.10.010

[20] Heiligers, J., Diedrich, B., Derbes, W., McInnes, C.: Sunjammer: Preliminary end-to-end mission design. In: AIAA/AAS Astrodynamics Specialist Conference. American Institute of Aeronautics and Astronautics, Reston, VA (2014). https://doi.org/10.2514/6.2014-4127

[21] Pezent, J.B., Sood, R., Heaton, A., Miller, K., Johnson, L.: Preliminary trajectory design for NASA's solar cruiser: A technology demonstration mission. Acta Astronautica **183**, 134–140 (2021) https://doi.org/10.1016/j.actaastro.2021.03.006

[22] Gong, S., Macdonald, M.: Review on solar sail technology. Astrodynamics **3**(2), 93–125 (2019) https://doi.org/10.1007/s42064-019-0038-x

[23] Hamilton, D.P., Burns, J.A.: Orbital stability zones about asteroids II. The destabilizing effects of eccentric orbits and of solar radiation. Icarus **96**(1), 43–64 (1992) https://doi.org/10.1016/0019-1035(92)90005-R

[24] Murray, C.D., Dermott, S.F.: Solar System Dynamics. Cambridge University Press, Cambridge (2000). https://doi.org/10.1017/CBO9781139174817

[25] Richardson, D.L.: Analytic construction of periodic orbits about the collinear points. Celestial Mechanics **22**(3), 241–253 (1980) https://doi.org/10.1007/BF01229511

[26] Gómez, G., Masdemont, J.J., Mondelo, J.M.: The dynamics around the collinear equilibrium points of the RTBP. Physica D **157**(4), 283–321 (2001) https://doi.org/10.1016/S0167-2789(01)00312-8

[27] Ceccaroni, M., Celletti, A., Pucacco, G.: Bifurcations thresholds of halo orbits. In: Astrodynamics Network AstroNet-II. Astrophysics and Space Science Proceedings, vol. 44, pp. 35–44. Springer, Cham (2016). https://doi.org/10.1007/978-3-319-23986-6_3

[28] Jorba, À., Masdemont, J.: Dynamics in the center manifold of the collinear points of the restricted three body problem. Physica D: Nonlinear Phenomena **132**(1-2), 189–213 (1999) https://doi.org/10.1016/S0167-2789(99)00042-1

[29] Ceccaroni, M., Celletti, A., Pucacco, G.: Halo orbits around the collinear points of the restricted three-body problem. Physica D: Nonlinear Phenomena **317**, 28–42 (2016) https://doi.org/10.1016/j.physd.2015.12.004

[30] Pucacco, G.: Structure of the centre manifold of the L_1, L_2 collinear libration points in the restricted three-body problem. Celestial Mechanics and Dynamical Astronomy **131**(10), 44 (2019) https://doi.org/10.1007/s10569-019-9922-4

[31] Bucciarelli, S., Ceccaroni, M., Celletti, A., Pucacco, G.: Qualitative and analytical results of the bifurcation thresholds to halo orbits. Annali di Matematica Pura ed Applicata **195**(2), 489–512 (2016) https://doi.org/10.1007/s10231-015-0474-2

[32] Celletti, A., Lhotka, C., Pucacco, G.: The dynamics around the collinear points of the elliptic three-body problem: A normal form approach. Physica D: Nonlinear Phenomena **468**, 134302 (2024) https://doi.org/10.1016/j.physd.2024.134302

[33] Breakwell, J.V., Brown, J.V.: The 'Halo' family of 3-dimensional periodic orbits in the Earth-Moon restricted 3-body problem. Celestial Mechanics **20**(4), 389–404 (1979) https://doi.org/10.1007/BF01230405

[34] Howell, K.C.: Three-dimensional, periodic, 'halo' orbits. Celestial Mechanics **32**(1), 53–71 (1984) https://doi.org/10.1007/BF01358403

[35] Doedel, E.J., Romanov, V.A., Paffenroth, R.C., Keller, H.B., Dichmann, D.J., Galán-Vioque, J., Vanderbauwhede, A.: Elemental periodic orbits associated with the libration points in the circular restricted 3-body problem. International Journal of Bifurcation and Chaos **17**(08), 2625–2677 (2007) https://doi.org/10.1142/S0218127407018671

[36] Mori, O., Sawada, H., Funase, R., *et al.*: First solar power sail demonstration by IKAROS. Transactions of the Japan Society for Aeronautical and Space Sciences **8**(ists27), 4–25431 (2010) https://doi.org/10.2322/tastj.8.To_4_25

[37] Tsuda, Y., Mori, O., Funase, R., Sawada, H., Yamamoto, T., Saiki, T., Endo, T., Kawaguchi, J.: Flight status of IKAROS deep space solar sail demonstrator. Acta Astronautica **69**(9–10), 833–840 (2011) https://doi.org/10.1016/j.actaastro.2011.06.005

[38] Spencer, D.A., Betts, B., Bellardo, J.M., Diaz, A., Plante, B., Mansell, J.R.: The LightSail 2 solar sailing technology demonstration. Advances in Space Research **67**(9), 2878–2889 (2021) https://doi.org/10.1016/j.asr.2020.06.029

[39] McNutt, L., Johnson, L., Clardy, D., Castillo-Rogez, J., Frick, A., Jones, L.: Near-Earth asteroid scout. AIAA SPACE Conference Proceedings (2014) https://doi.org/10.2514/6.2014-4435

[40] Wilkie, W.K.: The NASA advanced composite solar sail system (ACS3) flight demonstration. Technical Report NTRS 20210016824, NASA (2021)

[41] Japan Aerospace Exploration Agency: Small Solar Power Sail Demonstrator 'IKAROS' Confirmation of Photon Acceleration. Press release, 9 July 2010 (2010). https://www.jaxa.jp/press/2010/07/20100709_ikaros_e.html

[42] Aliasi, G., Mengali, G., Quarta, A.A.: Artificial periodic orbits around L1-type equilibrium points for a generalized sail. Journal of Guidance, Control, and Dynamics **38**(9), 1847–1852 (2015) https://doi.org/10.2514/1.G000904

Supplementary Files

This is a list of supplementary files associated with this preprint. Click to download.

- OnlineResource1derivations.pdf